Comparison and spatial profiling of strain in [001]- and [111]-oriented $In_xGa_{1-x}As/GaAs$ superlattices from Raman and x-ray experiments

U. D. Venkateswaran, T. Burnett, L. J. Cui, M. Li, and B. A. Weinstein
Department of Physics and Astronomy, State University of New York at Buffalo, 239 Fronczak Hall, Buffalo, New York 14260

H. M. Kim and C. R. Wie
Department of Electrical Engineering, State University of New York at Buffalo, Buffalo, New York 14260

K. Elcess and C. G. Fonstad
Department of Materials Science and Engineering, Massachusetts Institute of Technology, Cambridge, Massachusetts 02139

C. Mailhiot*
Xerox Corporation, Webster Research Center, Webster, New York 14580
(Received 5 February 1990)

We present spatial area maps of the built-in strain in [001]- and [111]-grown $In_xGa_{1-x}As/GaAs$ superlattices obtained from Raman studies, and strain depth profiles obtained from x-ray rocking-curve (XRC) studies on the same samples. A theory developed for Raman scattering under applied uniaxial stress has been used to determine the internal strain from the phonon frequency shifts with respect to the unstrained bulk constituents. It is shown that in two-component heterostructures exhibiting single-peak behavior, an overestimation or underestimation of the strain may result if the effects of strain and alloying do not compensate each other completely. For the $In_xGa_{1-x}As/GaAs$ system, we find that the average strain derived from the LO-phonon data compares well with the XRC results. But if the shift of the TO phonons in [111]-grown samples is used, an underestimate of the strain is found, which is explained by the above mechanism. Information about sample quality and strain variations related to growth are inferred from the strain maps.

I. INTRODUCTION

The possibility of exploiting lattice mismatch to achieve expanded engineering of device properties in epitaxially grown semiconductor quantum wells and superlattices has motivated immense activity in materials research in recent years.[1] Of particular interest here is the $GaAs/In_xGa_{1-x}As$ system, which has received considerable attention in both the fundamental and technological arenas. Smith and Mailhiot[2,3] predicted several novel nonlinear applications in this system based on pumped-carrier screening of the symmetry-allowed piezoelectric fields in [111]-oriented strained-layer superlattices (SLSL's). These strain fields stem from the rhombohedral distortion present for growth along this direction. Similar piezoelectric fields are expected for other low-symmetry growth axes, but not for the common [001] orientation. These recent predictions have been supported by various optical[4,5] and infrared[6] experiments.

The accurate measurement of the internal strain in mismatched heterostructures is clearly an important prerequisite to their characterization and controlled design. Several experimental techniques are available that give information about lattice-mismatch strain, including double-crystal x-ray rocking-curve (XRC),[7] Rutherford backscattering (RBS) and channeling,[8] electron microscopy, and Raman spectroscopy.[9] The problem of determining the internal strain is complicated for growth directions other than [001] because detailed interface-dislocation models describing the critical thickness for perfect epitaxial growth are not well developed for arbitrary directions of growth.

In a recent paper, we discussed the determination and spatial mapping of the built-in strain in [001]- and [111]-oriented $In_xGa_{1-x}As/GaAs$ SLSL's by Raman scattering. In the present paper we elaborate on the details of both the Raman and XRC techniques, presenting high-density areal strain maps, and strain depth profiles. We find that the combined results of both techniques present a comprehensive characterization of the internal strain. Raman scattering is a relatively gentle and rapid method for directly measuring the elastic strain in each constituent layer. Also, it offers a practical method for producing areal strain maps of macroscopic films.[10] Although the achievable scale is much coarser than that obtained with shorter-wavelength probes, it is particularly helpful for characterizing grain-size and larger imperfections, and nonuniformities from deposition angles, temperature gradients, flow-rate variations, and other practical growth considerations. For its part, XRC can provide direct information on the in-plane and plane-normal lattice constants and their mismatch for the constituents in a SLSL. In addition, layer thickness, compositions, and the depth profile of elastic strain in the presence of a buffer layer can be inferred by analyzing XRC data.

The experimental details of both the Raman setup and

the XRC technique are described in Sec. II. The Raman results are discussed in Sec. III, where we outline the method of evaluating the internal strain from phonon frequency shifts and present spatial maps of the strain in both the GaAs and $In_xGa_{1-x}As$ layers. In Sec. IV we describe the XRC measurements and their analysis. A comparison of the Raman and XRC results is presented in Sec. V. We find that meaningful Raman strain measurements hinge on assessing the competing effects of alloying and strain for every phonon-mode type and every growth orientation, particularly when single-peak behavior is observed in a SL (the present case). Finally, the potential usefulness of Raman strain maps combined with XRC results, in characterizing epitaxial samples with nonconventional growth orientations, is also discussed.

II. EXPERIMENTAL DETAILS

The three $In_xGa_{1-x}As/GaAs$ SLSL's studied here were grown by molecular-beam epitaxy (MBE) and characterized as previously described.[5,11] Their growth parameters are given in Table I. All three superlattices were grown on semi-insulating GaAs substrates with graded buffer layers designed such that the strain conditions would correspond to those of zero net strain, or "free-standing" superlattices. Samples 1 and 2 were grown simultaneously, situated next to each other in the MBE chamber, and therefore they should be directly comparable except for their different orientations. Sample 3 was grown separately with a higher In concentration.

Raman scattering was excited with ~20 mW of 4825-Å Kr^+-laser radiation focused into a ~10-μm spot and incident normal to the sample plane. Backscattering spectra were recorded using a custom-built Raman microprobe having 250× magnification and 50 mm working distance, and a standard double-grating (1800 grooves/mm) monochromator with an image-intensified 700-Si-diode array detector and microcomputer control. An integration time of ~250 sec yielded a 20:1 signal-to-noise ratio, sufficient to achieve an accuracy of ±0.3 cm^{-1} in the phonon frequency. These frequencies were determined by fitting Lorentzian profiles to the Raman peaks. All measurements were performed at ~300 K; no laser-heating-induced phonon shifts could be observed for laser powers <25 mW. The samples could be reproducibly positioned to ±0.5 μm accuracy in the laser focal plane by computer-controlled x-y stages. For samples 1 and 2, a semiautomated procedure was used to record spectra in spatial clusters of three points separated by 30 μm, with ~2.0 mm between each cluster. Higher-density maps for sample 3 were obtained by probing an area of ~5.5×5 mm^2 with a uniform point separation of 500 μm using a recently developed computer-controlled system that is completely automated.[12] By employing near-real-time curve fitting to avoid the large memory requirements of high-density Raman mapping, automated mapping at a rate of 50 points/h is achieved with a standard Motorola 68-286-level IBM AT-compatible computer.

Double-crystal XRC patterns were obtained using Fe $K\alpha_1$ radiation diffracted from an [001] GaAs first crystal. The incident x-ray beam had a cross section of ~1×1 mm^2 at the sample, defined by a slit placed after the first crystal, which also eliminated the $K\alpha_2$ line. The samples were placed on a goniometer which rotated at an angular step of ~0.001°. Up to six XRC's were recorded for each sample. For the [001]-oriented sample, (004) and two (224) reflections (at large and small angles of incidence) were chosen, and, for the [111]-grown samples, (333) and two (224) reflections were used. After the first series of measurements, the sample was rotated by 180° about the surface normal, and XRC's at the above reflections were recorded again. Results from the same reflection for the two positions of the sample were averaged to cancel out possible crystallographic misorientation between the epitaxial layer and the substrate.[13]

III. PHONON DATA AND RESULTS

A. Raman spectra

Figure 1 shows the Raman spectra of samples 1–3 recorded for the ($\|,\|$) polarization geometry. Solid and dashed vertical arrows denote the frequency positions of the phonons in unstrained GaAs and unstrained $In_xGa_{1-x}As$, respectively. Note that only a single

TABLE I. Nominal growth parameters of the SLSL's under study. x, d, and n refer to In concentration, thickness, and repetition number, respectively.

Sample no.	Orientation	Parameter	GaAs barrier	In-Ga-As well	Buffer layer(s)	
1	[001]	x	0.0	0.1	0→0.03	
		d (Å)	140	70	3000	
		n	21	20	1	
2	[111]B	x	0.0	0.1	0→0.03	
		d (Å)	140	70	3000	
		n	21	20	1	
					B_1	B_2
3	[111]B	x	0.0	0.17	0→0.06	0
		d (Å)	140	70	15 000	5000
		n	21	20	1	1

GaAs-like LO-phonon peak (for [001] growth, sample 1), or a single LO-TO pair (for [111] growth, samples 2 and 3), is observed in the spectra of the SLSL's. Each peak occurs at a frequency shifted from its bulk unstrained counterparts. The appearance of only single LO- and TO-phonon peaks in the presence of two constituents (we shall call this "single-peak" behavior), whose GaAs-like phonons differ by a few cm^{-1} in the bulk, is not due to poor instrumental resolution. (See the indicated slit width in Fig. 1). Single LO- and TO- phonon peaks have been observed repeatedly in this materials system for [001]-grown epitaxial films and SL's with $x<0.2$.[9,10,14–16]

We find that the Raman spectra of all three samples closely obey bulklike backscattering selection rules, viz., for [001] orientation, the LO mode is forbidden for scattering depolarized with respect to (110) and the TO mode is always forbidden, and for [111] orientation the LO mode is forbidden for scattering depolarized with respect to $(11\bar{2})$ and LO *and* TO modes are otherwise allowed. Since scattering from interface and higher-order confined modes obeys different selection rules,[9] we find that these modes do not contribute appreciably to our spectra, a result expected for the nonresonant laser excitation used in our experiments. Phonon-confinement effects are also not significant because of the relatively large layer thicknesses in the SLSL's studied here. Therefore, the Raman spectra like those shown in Fig. 1 can be used to evaluate local strain in the SL layers using the same theoretical model that applies to strain in bulk materials.

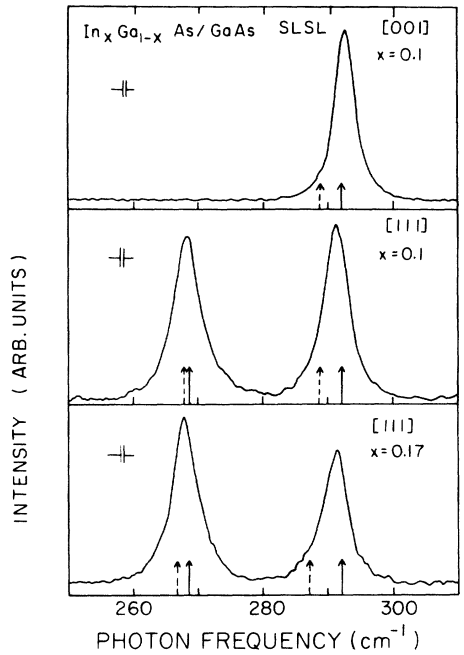

FIG. 1. Raman spectra of [001]- and [111]-oriented $In_xGa_{1-x}As/GaAs$ SLSL's. Solid and dashed arrows indicate the phonon frequency positions in the GaAs and $In_xGa_{1-x}As$ unstrained bulk constituents, respectively.

B. Calculation of internal strain

A theory originally developed to treat applied uniaxial stress in bulk semiconductors[17] can be used to evaluate the local elastic strain within the layers of a SLSL. In this theory, one expands the effective phonon spring constants K_{ik} linearly in the strain components ϵ_{lm} and then solves the resulting secular equation as in degenerate perturbation theory to first order in the strain. For zinc-blende-type materials, the solution can be cast in terms of the three independent components of a dimensionless fourth rank tensor $\tilde{K}_{ij}$ (in contracted notation), which are known from applied-stress measurements.[9] The scattering geometry determines the LO and TO strain-singlet or strain-doublet character of the eigenfrequencies; any variation of the LO-TO splitting due to strain can then be included via different $\tilde{K}_{ij}$ values. The calculated expressions relating the in-plane strain ϵ_p to the induced frequency shifts $\Delta\omega$ of the allowed phonons measured in backscattering for [001]- and [111]-growth axes are

$$(\Delta\omega/\omega)_{\mathrm{LO}} = \tfrac{1}{2}[(\tilde{K}_{11}+2\tilde{K}_{12})-\tilde{K}_{11}(1+\Gamma)]\epsilon_p, \quad [001]\ \text{growth} \tag{1}$$

$$(\Delta\omega/\omega)_{\left\{\substack{\mathrm{LO}\\ \mathrm{TO}}\right\}} = \tfrac{1}{6}[(\tilde{K}_{11}+2\tilde{K}_{12})(2-\Gamma)+\left\{\substack{-4\\ +2}\right\}\times\tilde{K}_{44}(1+\Gamma)]\epsilon_p, \quad [111]\ \text{growth}\ . \tag{2}$$

Here, Γ relates the in-plane and plane-normal strain components according to $\epsilon_n=-\Gamma\epsilon_p$. The appropriate expressions for Γ are

$$\Gamma=2\frac{C_{12}}{C_{11}}, \quad [001]\ \text{growth} \tag{3}$$

$$\Gamma=2\frac{C_{11}+2C_{12}-2C_{44}}{C_{11}+2C_{12}+4C_{44}}, \quad [111]\ \text{growth} \tag{4}$$

where the C_{ij} are elastic constants. Equations (1)–(4) are to be applied separately to each constituent of a SLSL. As expected from the first-order perturbation treatment, Eqs. (1) and (2) give a linear relationship between ϵ_p and $\Delta\omega$. Cast in a convenient form for later tabulation, these equations read

$$\epsilon_p=\alpha\,\Delta\omega\ , \tag{5}$$

where we note that the parameter α is a constant that depends on the material, growth direction, and phonon-mode type.

Use of Eqs. (1)–(4) is straightforward for SLSL's like Si/Ge, in which two distinct phonon peaks corresponding to each of the constituents are observed.[9] However, for SLSL's exhibiting single-peak behavior, it is impor-

tant to examine the effects of strain and alloying on the phonon frequencies. In general, there would be three cases, as illustrated in the top portion of Fig. 2. Here, vertical solid arrows refer to the frequency positions of the phonons in the corresponding unstrained bulk materials which we denote as $\omega_0^{(1)}$ and $\omega_0^{(2)}$; superscripts (1) and (2) refer to the two constituents. For a given internal strain due to lattice misfit in the SL, the phonon frequencies shift by amounts $\Delta\omega$ given by Eqs. (1)–(4) (represented by the horizontal arrows in Fig. 2) and would thus appear at $\omega_s^{(1)}$ and $\omega_s^{(2)}$. The single-peak frequency ω observed in the SLSL will then lie at a centroid position determined by weighting $\omega_s^{(1)}$ and $\omega_s^{(2)}$ in proportion to the layer thickness of materials (1) and (2), respectively. Figure 2(a) depicts the case where the strain-induced phonon frequency shifts in the two constituents exactly compensate the effect of alloying. In that case both frequencies coincide, resulting in a single peak, i.e., $\omega_s^{(1)}=\omega_s^{(2)}=\omega$. Figures 2(b) and 2(c) represent cases where the strain-alloying compensation is not complete. In Fig. 2(b) the strain-induced frequency shifts are large, and so the use of Eqs. (1)–(4) with a single observed peak

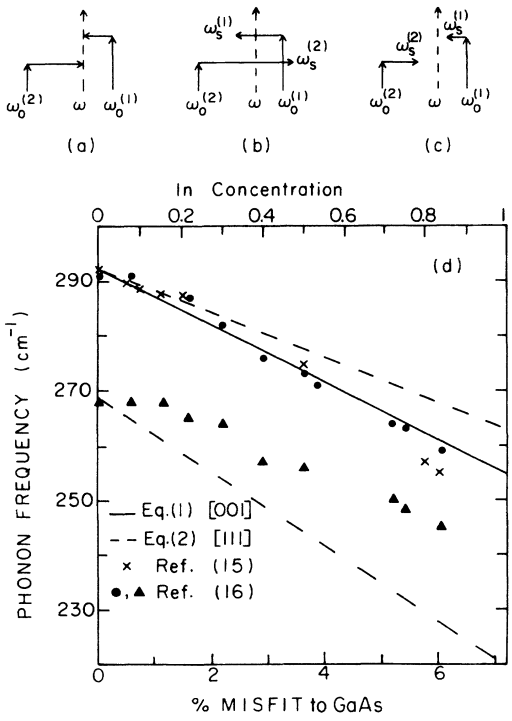

FIG. 2. Top: Illustration of the three cases that arise in a SLSL showing single-peak behavior. Vertical solid arrows at $\omega_0^{(1,2)}$ refer to the phonon frequencies in unstrained bulk materials. Horizontal arrowheads are at the strain-shifted phonon frequency positions, $\omega_s^{(1,2)}$. Dashed vertical arrows at ω give the expected Raman-peak centroid in the SLSL. Cases (a), (b), and (c) represent situations where the strain-induced shift is equal to, more, or less than that due to In concentration in bulk alloys, respectively (see text). (d) Plot of LO- and TO-phonon frequencies in $In_xGa_{1-x}As$ alloy vs In concentration (top axis) and corresponding misfit strain with respect to GaAs (bottom axis).

frequency at ω will result in an underestimate of the strain. The opposite situation prevails in Fig. 2(c) and will lead to an overestimate of the strain.

Let us verify which of the cases discussed above applies to the $In_xGa_{1-x}As/GaAs$ system. To do this, we plot in Fig. 2(d) the LO- and TO-phonon frequencies that have been measured in unstrained bulk $In_xGa_{1-x}As$ alloys[15,16] versus the indium composition of these alloys x (top axis), or, equivalently, the misfit strain f with respect to GaAs (bottom axis). The strain-induced phonon frequencies that would be predicted by Eqs. (1)–(4) for strains appropriate to [001]- and [111]-growth axes are given by the solid and dashed lines, respectively. It can be seen that for LO phonons in [001]-grown SLSL's the frequency shifts due to strain and alloying fall virtually on the same line. This means that the single observed LO phonon frequency in [001] SLSL's will determine the strain in both of the constituent layers accurately. However, for the LO phonons in [111]-grown SLSL's, complete strain-alloying compensation holds only when $f<2\%$ or $x<0.27$. Furthermore, for the TO phonons the frequency shift with alloying is always smaller than that due to strain. This implies that in the [111]-grown $In_xGa_{1-x}As/GaAs$ SLSL's a situation similar to that shown in Fig. 2(a) exists for the LO phonons when $x<0.27$, but the case depicted in Fig. 2(b) applies for the TO phonons at all compositions. Therefore, the LO-phonon data will describe the internal strain accurately for the samples studied here, while the TO-phonon data should underestimate the strain. Very recent studies of several [112]-grown $GaAs/In_xGa_{1-x}As$ $(0.1<x<0.2)$ SLSL's yield similar results.[18]

C. Mapping results

The internal strains within the SLSL layers of our samples were calculated from the measured phonon frequency shifts $\Delta\omega$ using Eqs. (1)–(4) and the appropriate scaling coefficients α. The unstrained reference frequencies were taken for GaAs from our own measurements, and for $In_xGa_{1-x}As$ from a best fit (standard deviation ±0.5 cm^{-1}) to previous data on bulk alloys for $0<x<0.3$.[15,16] Table II lists the values of α and of the spatially averaged phonon frequency shifts for both the LO and TO phonons in the three samples studied. In Fig. 3 we display the measured spatial area maps of the internal strain derived from the LO-phonon data of sample 1 ([001] growth) and sample 2 ([111] growth). The data are represented by tetrahedra connected to the x-y plane (containing the sample outline) by vertical lines whose heights give the measured in-plane strains ϵ_p; the left- and right-hand scales describe ϵ_p in the GaAs and $In_{0.1}Ga_{0.9}As$ layers, respectively. Note the sign change due to the tension in the former and compression in the latter. The occurrence of a single LO-phonon peak in the spectra assures that ϵ_p in both constituents can be represented on the same diagram. The dashed line above the x-y plane gives the areally averaged strain (also listed in Table III), useful for comparison to the x-ray rocking-curve results. An uncertainty in ϵ_p of ±0.05 arises from our ±0.3 cm^{-1} peak-location uncertainty. An additional

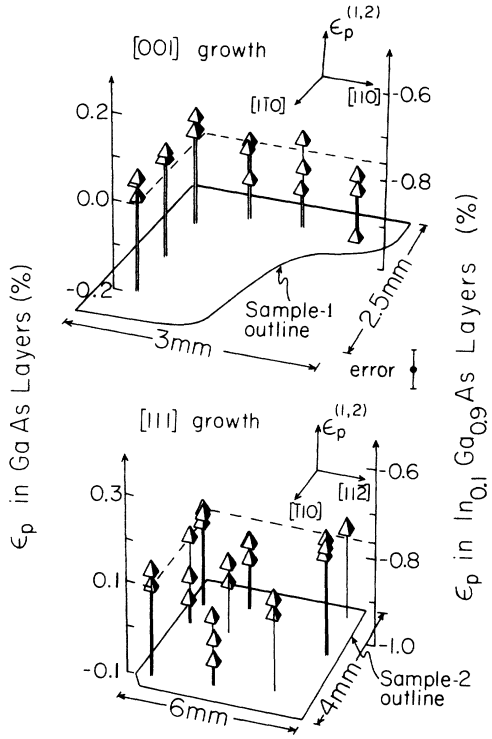

FIG. 3. Maps of internal strain in [001]- and [111]-oriented $In_{0.1}Ga_{0.9}As/GaAs$ SLSL's (samples 1 and 2). Dashed line represents the areal average of the strain in GaAs and In-Ga-As layers, according to the left- and right-hand vertical scales, respectively.

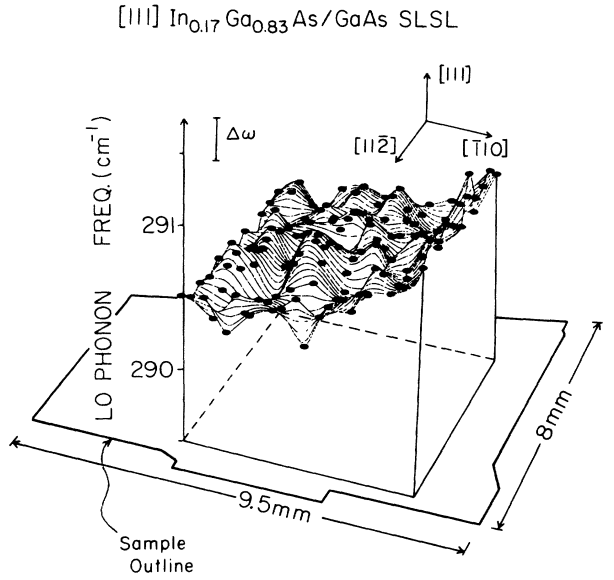

FIG. 4. High-density spatial map of the LO-phonon frequency in [111]-oriented $In_{0.17}Ga_{0.83}As/GaAs$ SLSL (sample 3). Observe the systematic increase of the frequency along the [$\bar{1}$10] axis. Solid dots are data; contour lines are best-fit computer interpolations between points.

uncertainty of similar size also can arise from the experimental accuracy of the unstrained bulk frequencies used. The former contribution is the principal inaccuracy for mapping relative spatial variations of strain, while the latter needs to be included in determining the absolute strain. The error flag in Fig. 3 shows the point-to-point mapping inaccuracy arising from the peak-location uncertainty in the present measurements.

It can be observed that for both samples 1 and 2 ($x=0.1\%$) ϵ_p is uniform on a 30 μm scale, but varies over macroscopic dimensions. Sample 1 shows a decrease in ϵ_p along the [110] direction, and sample 2 has a variation along [11$\bar{2}$] showing more compression in the middle of the sample compared to the edges. The similar magnitude and spatial extent of the strain variations in samples 1 and 2 are expected since both samples were grown simultaneously. The maps presented in Fig. 3 demonstrate that small, systematic variations in strain over the sample area are easily discerned by the Raman technique.

For sample 3, which is a [111]-oriented SLSL with a higher In concentration ($x=0.17$) and, consequently, a larger lattice mismatch, we recorded high-density spatial maps using the completely automated scanning system described above. Figure 4 is the map of the measured LO-phonon frequency at various positions on the sample. The solid circles on the contour lines are the actual data points taken at 500-μm intervals in the x and y directions. The corresponding strain map shown in Fig. 5 is obtained by scaling Fig. 4 with the appropriate value of α calculated according to Eq. (2) and given in Table II. In this

TABLE II. Average strain-induced phonon frequency shifts ($\Delta\omega$) and the scaling factor α connecting ϵ_p and $\Delta\omega$ via Eq. (5).

Sample no.	SL layer type	$\Delta\omega$ (cm^{-1}) LO	$\Delta\omega$ (cm^{-1}) TO	α (cm) LO	α (cm) TO
1	GaAs	−0.02		−0.19	
	$In_{0.1}Ga_{0.9}As$	3.82		−0.199	
2	GaAs	−0.28	−0.48	−0.248	−0.146
	$In_{0.1}Ga_{0.9}As$	2.90	0.81	−0.262	−0.149
3	GaAs	−1.50	−0.75	−0.248	−0.146
	$In_{0.17}Ga_{0.83}As$	3.60	1.45	−0.275	−0.152

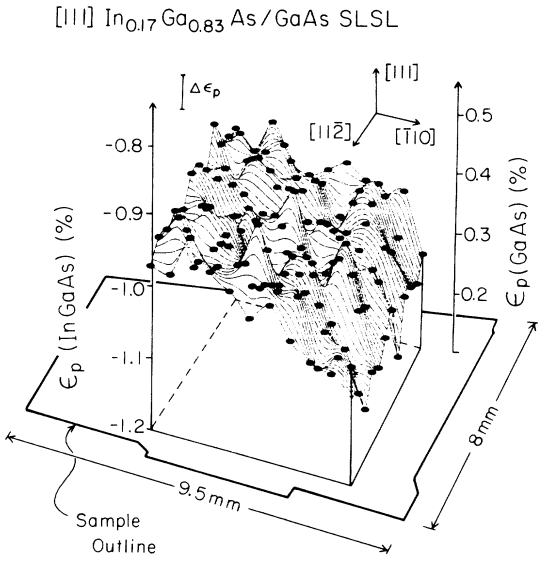

FIG. 5. Areal map of the internal strains in the GaAs and $In_{0.17}Ga_{0.83}As$ layers of sample 3 derived from the frequency map in Fig. 4 using Eq. (5) with α given in Table II.

sample we also observe a systematic decrease in ϵ_p over macroscopic distances along the [$\bar{1}$10] direction.

IV. XRC ANALYSIS

XRC experiments on epitaxial films[7,19] study the extended angular profiles of selected diffraction spots. Hence, they directly measure the deviations from the substrate of whatever average interplanar spacings exist in the film corresponding to these reflections. This is often called the x-ray strain ($\epsilon^{\text{x-ray}}$). Two reflections, one symmetric and another asymmetric with respect to the sample plane, are required to obtain both the average in-plane and plane-normal lattice constants a_p and a_n. The symmetric diffraction yields a_n, and the asymmetric one with large incidence angle gives a mixture of a_p and a_n which must be deconvoluted in the analysis. For pseudomorphic growth in SL's, $a_p = a_p(1) = a_p(2)$, but $a_n \neq a_n(1) \neq a_n(2)$ because of the tension and compression in alternate layers. To extract these lattice constants accurately, the measured rocking curves are fitted using dynamical diffraction theory.[7] The elastic strains for each SL layer are obtained from

$$\epsilon_{(n,p)} = \epsilon^{\text{x-ray}}_{(n,p)} - \epsilon_f \ , \tag{6}$$

where ϵ_f is the mismatch of the film lattice constant for the particular SL layer under consideration with respect to the substrate.[13]

In our experiments another (224) reflection with a small incident angle was used to check the consistency of the fitted parameters obtained from the other two reflections, viz., (004) and (224) in sample 1 and (333) and (224) in samples 2 and 3, where this (224) reflection was taken with a large incident angle. The fitting algorithm took into account buffer-layer and higher-order superlattice contributions in addition to the substrate and principal superlattice peaks. In this way a depth profile corresponding to the different stages of growth could be obtained. The fitting depends on several parameters, and, in particular, the elastic strain in the $In_xGa_{1-x}As$ layers depends interactively on the ratio of the layer thickness $h^{(1)}/h^{(2)}$ and on the In composition x.

Figure 6 shows the experimental (dots) and the best-fit simulated (solid lines) rocking curves for samples 1–3. Here, we only show the symmetric (004) reflection for sample 1 in Fig. 6(a), and the large-angle-incidence asymmetric (224) reflection for samples 2 and 3 in Figs. 6(b) and 6(c), respectively. The quality of the fit was the same in each of the other XRC's. Note that only those superlattice peaks with the highest peak-reflecting power appear clearly in the experimental curves. This is probably due to degraded SL layer quality since we find that a random fluctuation in the SL period affects the relative intensities of the XRC peaks and the background significantly.[20] The solid lines in Figs. 6(a) and 6(c) include 30% and 10% variations in the layer thicknesses of samples 1 and and 3, respectively. Because of the effect of such variations, the SL strains, indium concentrations, and layer thicknesses are determined from fitting the XRC peak positions rather than the peak intensities. Figure 6(b) demonstrates the sensitivity of this procedure by comparing the fits corresponding to two slightly different strains on the XRC peak positions. The solid line is the calculated XRC for in-plane and plane-normal

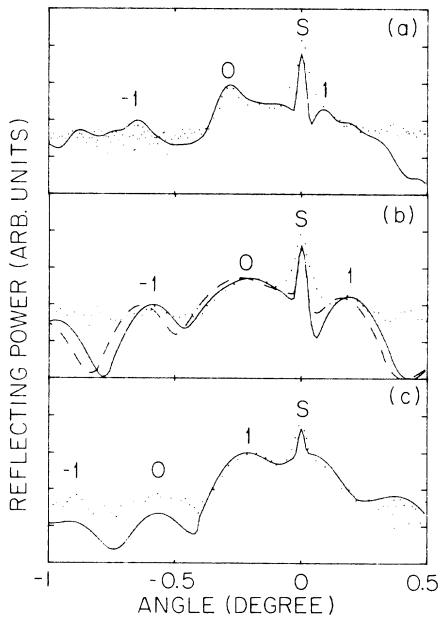

FIG. 6. Experimental (dots) and best-fit calculated (solid curves) XRC's. The substrate, zeroth-, and first-order SL peaks are denoted by S, 0, and ± 1, respectively. (a) (004) reflection for sample 1; calculated XRC includes a 30% random fluctuation in the SL layer thicknesses. (b) (224) reflection for sample 2. Solid and dashed curves correspond to strain differences of $\sim 0.04\%$ (see text). (c) (224) reflection for sample 3; calculated XRC allows for a 10% random fluctuation in the thickness.

TABLE III. Comparison of the percentage in-plane strain (ϵ_p) measured by XRC and Raman experiments in samples 1–3. Values expected in corresponding free-standing (FS) SL's are also given. Indium composition (x) and layer thickness (h) given here are the *best-fit values* from the XRC analysis. (See discussion in text).

Sample no.	SL layer type	x (%)	h (Å)	ϵ_p (%) XRC	Raman	FS
1	GaAs	0.0	128	0.007	−0.004 (LO)	0.26
	In-Ga-As	10.8	64	−0.77	−0.76 (LO)	−0.53
2	GaAs	0.0	126	0.14	0.10 (LO)	0.22
					0.07 (TO)	
	In-Ga-As	9.0	63	−0.51	−0.76 (LO)	−0.43
					−0.12 (TO)	
3	GaAs	0.0	132	0.33	0.37 (LO)	0.41
					0.11 (TO)	
	In-Ga-As	17.5	106	−0.93	−0.99 (LO)	−0.82
					−0.22 (TO)	

lattice mismatches of 0.138% and 1.132%, respectively. The dashed line is the calculated XRC corresponding to values of 0.11% and 1.16% for the parallel and perpendicular mismatches with all other parameters unchanged from the previous solid-curve result. Even without improving the fit by including layer-thickness fluctuations, the significant difference in the agreement with the experimental data establishes the accuracy of our method for extracting the strain from the XRC data. We find that the expected XRC strain uncertainty is $\sim\pm0.05$ in the percentage strain values, similar to that obtained by the Raman technique. The best-fit XRC values of the layer thicknesses, indium concentrations, and the in-plane elastic strains are given in Table III for all three samples. The x-ray strain depth profiles resulting from these fits are presented in Fig. 7. The solid lines represent the normal mismatch $(a_n - a_s)/a_s$ and the dashed lines represent the parallel mismatch $(a_p - a_s)/a_s$, where a_s is the substrate lattice constant.

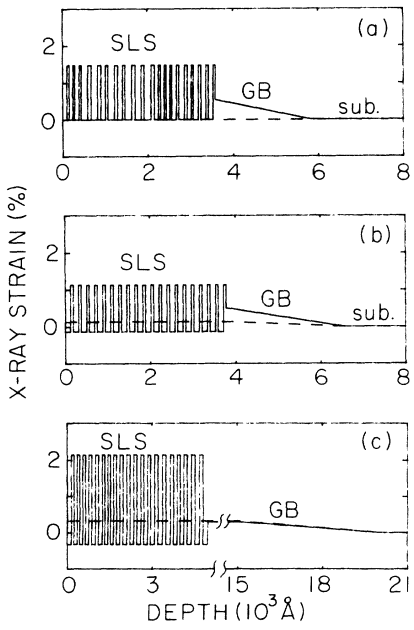

FIG. 7. Depth profiles of in-plane (dashed) and plane-normal (solid) *x-ray strains* within the constituent layers and graded-buffer (GB) regions of samples 1, 2, and 3, shown in (a), (b), and (c), respectively.

V. DISCUSSION

The areal averages of the Raman measured strains in samples 1–3 obtained from the shift of *both* the LO- and TO-phonon peaks are listed in Table III for comparison with the XRC results. Averaging of the Raman data is necessary for this comparison because the x-ray measurements probed a 1-mm^2 area at an undetermined position of the samples. Note that the best-fit XRC results vary only slightly from the nominal growth values (see Table I) of the layer widths and In compositions. Table III shows that the best-fit XRC strains, when converted to elastic strains, agree within experimental uncertainty with the corresponding Raman LO-phonon average strains. We regard this independent agreement between the Raman-LO and XRC strains to be quite satisfactory considering the complicated graded buffer substructure in our samples and the small values of x leading to small strains.

In contrast to the LO-phonon results, the Raman-measured strains obtained from the shift of the TO phonons tend to be smaller by a factor of 2. As we discuss further below, this is a consequence of the occurrence of one-peak behavior at small x *and* of the lack of exact compensation between the effect of mismatch-induced strain and that of alloying for the TO frequency.

The occurrence of single GaAs-like peaks is an interesting aspect of the $In_xGa_{1-x}As/GaAs$ system that has been investigated for [001]-oriented $x < 0.27$ material.[9,14,21] Although not completely understood, it is related to the frequency overlap between the *internal-strain-*

shifted GaAs-like optical branches in each SL constituent. If, for a given mode and growth orientation, the compensation of misfit strain and alloying is complete, then the GaAs-like phonons from each SL constituent become degenerate and appear as a single Raman peak. This degeneracy results because the compressive stress in the GaAs layers and the tensile stress in the $In_xGa_{1-x}As$ layers shift their respective phonon frequencies in opposite directions, thereby bringing them into coincidence. Then the single-peak centroid frequency reflects the true shift from the unstrained bulk frequency of *each* SL constituent. This is the situation depicted in Fig. 2(a). As we have argued, it applies to LO phonons in this materials system for [001] and [111] SLSL's with $x<0.27$. [See Fig. 2(d).]

On the other hand, even if the compensation between the effects of strain and alloying is incomplete, the strain-shifted optical-phonon frequencies of the two constituents can still be close enough to come within the intrinsic Raman linewidth given by the inverse phonon lifetime. Under these conditions, a single symmetric phonon peak will still be expected in a SLSL. For example, the strain-shifted ω_{TO} frequencies of GaAs and $In_{0.17}Ga_{0.83}As$ for misfit biaxial strain corresponding to [111] growth differ by only ~ 6 cm^{-1} compared to the 5.5-cm^{-1} width of the observed TO peak. Hence, the single peak observed for sample 3 (see Fig. 1) is not surprising. Now, however, a situation such as that shown in Fig. 2(b) prevails, and the peak centroid does not accurately represent strain-induced effects in either constituent.

The phonon peak width will be determined by several factors. These involve the range of **q**-scattered needed to take into account the disorder due to chemical (e.g., alloying) and structural (e.g., dislocations) inhomogeneities, as well as that needed for thermal decay. These effects are not easily separated even in bulk $In_xGa_{1-x}As$, which exhibits one-mode alloy behavior for $x \lesssim 0.27$.[16,22] The situation is more complicated in SL's where interface dislocations, interlayer diffusion during growth, and phonon coupling between layers may play a part. Hence, further investigation of these issues is warranted, perhaps by high-resolution cryogenic measurements under uniaxial stress.

Another interesting issue for SLSL's is whether the bulk values of $\tilde{K}_{ij}$ in Eqs. (1) and (2) remain appropriate, especially for very thin layers (~ 25 Å) where interface forces become significant. Our experiments indicate that for [111]-oriented SLSL's the bulk $\tilde{K}_{ij}$ can be used to determine the strain within each constituent from measurements of the shift (from its bulk position) of the LO phonon, but not the TO phonon. We do not think that this discrepancy is due to the inappropriateness of using the bulk $\tilde{K}_{ij}$ for TO phonons, but rather to the lack of complete compensation between strain and alloying as explained above. Although modifications to the $\tilde{K}_{ij}$ remain a possibility, we expect this to be a higher-order effect.

The results presented in Table III allow an assessment of several sample characteristics related to growth. In each of the three SLSL's the measured GaAs strains obtained from both the Raman LO and XRC studies are lower than what is expected for free-standing growth. This indicates that the graded buffer layers, designed to achieve a free-standing SLSL, are In-deficient. In fact, the XRC analysis yielded a value of $x=0.044$ for the buffer layer in sample 3 instead of the intended value of 0.06. Secondary-ion-mass-spectroscopy and Rutherford-backscattering studies on sections from the same parent SLSL's also support this conclusion.[5,23]

For pseudomorphic growth of elastically similar materials on a substrate or buffer layer, ϵ_p is expected to be given by[1]

$$\epsilon_p^{(1,2)}=\pm\frac{h^{(2,1)}}{h^{(1)}+h^{(2)}}f+\bar{\epsilon}_s \ , \tag{7}$$

where the superscripts (1,2) label the constituents, h is the layer width, f the bulk misfit, and $+$ applies to constituent (1) (here GaAs). The first term on the right-hand side is the strain for a free-standing SL, and $\bar{\epsilon}_s$ is the net residual strain due to the substrate, or buffer in our case. We compute $\bar{\epsilon}_s$ from the Raman-measured $\epsilon_p^{(1,2)}$ assuming that the individual SL layers do not exceed their critical thickness h_c. This assumption is reasonable since h_c is measured to be ~ 1500 Å for $In_{0.1}Ga_{0.9}As$ films grown on GaAs substrates.[15] We find that $\bar{\epsilon}_s \lesssim -0.25\%$ for each SLSL. This is small compared to the maximum absolute misfits of 0.72% and 1.22% permissible for our $x=0.1$ and 0.17 samples, respectively. Hence, by any of the currently used estimates,[1] the 4200-Å thickness of these SLSL's should not exceed pseudomorphic limits. This is confirmed by recent transmission-electron-microscopy characterization, which shows that threading dislocations are well confined to the buffer regions.[5,23] Lastly, we remark that because $\bar{\epsilon}_s \neq 0$ the piezoelectric fields in these [111]-oriented SLSL's may differ in absolute magnitude from that expected for the free-standing case. The effect of a nonzero net strain on the special electronic and optical properties of [111]-oriented SLSL's has not been treated so far, and it would be of interest to consider this for the extreme, but perhaps functionally more common, case of unbuffered growth on GaAs.

VI. SUMMARY

A combination of Raman and XRC techniques has been used to obtain comprehensive spatial maps and depth profiles characterizing the internal strain in [001]- and [111]-grown $In_xGa_{1-x}As$/GaAs SLSL's. It is pointed out that for SLSL's exhibiting single-peak behavior it is important to examine the phonon frequency shifts due to the competing effects of chemical alloying and biaxial strain. In the $In_xGa_{1-x}As$/GaAs system the TO-phonon frequency shift with indium composition is always smaller than that due to misfit strain for the growth orientations studied here. Use of the TO Raman frequency will then result in an underestimate of the strain in each SL layer. On the other hand, it is shown by comparison with independent x-ray rocking-curve measurements on the same samples that the Raman LO data lead to an accu-

rate determination of the internal strain for [001] and [111] SLSL's with $x < 0.27$. Furthermore, the local and nondestructive nature of the Raman probe permits high-density mapping of the strain with micrometer resolution over macroscopic dimensions of the sample. We found evidence for pseudomorphic growth with some macroscopic inhomogeneities in the three SLSL's studied, which included both unconventional [111]- and conventional [001]-growth orientations. In combination, the spatial area maps obtained from Raman and the strain depth profiles obtained from XRC measurements have yielded a comprehensive three-dimensional picture of growth-related strain characteristics of the SLSL's studied.

ACKNOWLEDGMENTS

The authors are grateful to D. L. Smith and B. K. Laurich for many helpful discussions. One of us (B.A.W.) wishes to thank the Xerox Webster Research Center for supporting this work. Partial support for the work done at SUNY at Buffalo was also provided by the U.S. Office of Naval Research under Grant No. N00014-89-J-1797, the U. S. National Science Foundation (NSF) under Grant No. DMR-88-57403, and the University Center for Electronic and Electro-optic Materials; work at the Massachusetts Institute of Technology was supported by NSF Grant No. DMR-84-18718 through the Materials Science and Engineering Center.

*Present address: Lawrence Livermore National Laboratory, Livermore, CA 94550.

[1]See the review article by E. P. O'Reilly, Semicond. Sci. Techol. **4**, 121 (1989).

[2]D. L. Smith and C. Mailhiot, Phys. Rev. Lett. **58**, 1264 (1987); C. Mailhiot and D. L. Smith, Phys. Rev. B **35**, 1242 (1987).

[3]D. L. Smith and C. Mailhiot, J. Vac. Sci. Technol. A **5**, 2060 (1987).

[4]B. K. Laurich, K. Elcess, C. G. Fonstad, J. G. Beery, C. Mailhiot, and D. L. Smith, Phys. Rev. Lett. **62**, 649 (1989).

[5]J. G. Beery, B. K. Laurich, C. J. Maggiore, D. L. Smith, K. Elcess, C. G. Fonstad, and C. Mailhiot, Appl. Phys. Lett. **54**, 233 (1989).

[6]B. S. Yoo, X. C. Liu, A. Petrou, J. P. Cheng, A. A. Reeder, B. D. McCombe, K. Elcess, and C. G. Fonstad, Superlatt. Microstruct. **5**, 363 (1989); R. Ranganathan, B. S. Yoo, Y. J. Wang, B. D. McCombe, K. Y. Lim, F. Kuchar, K. Elcess, and C. Fonstad, Surf. Sci. **228**, 156 (1990).

[7]C. R. Wie, T. A. Tombrello, and T. Vreeland, Jr., J. Appl. Phys. **59**, 3743 (1986).

[8]K. M. Yu and K. T. Chan, Appl. Phys. Lett. **56**, 45 (1990).

[9]See B. Jusserand and M. Cardona, in *Light Scattering in Solids V*, Vol. 66 of *Topics in Applied Physics*, edited by M. Cardona and G. Güntherodt (Springer, New York, 1989).

[10]U. D. Venkateswaran, L. Cui, M. Li, B. A. Weinstein, K. Elcess, C. G. Fonstad, and C. Mailhiot, Appl. Phys. Lett. **56**, 286 (1990).

[11]K. Elcess, J. L. Lievin, and C. G. Fonstad, J. Vac. Sci. Technol. B **6**, 638 (1988).

[12]T. Burnett (unpublished).

[13]C. R. Wie, H. M. Kim, and K. M. Lau, Proc. SPIE Microoptoelectron. Mater. **877**, 41 (1988).

[14]F. Iikawa, F. Cerdeira, C. Vazquez-Lopez, P. Motisuke, M. A. Sacilotti, A. P. Roth, and R. A. Masut, Solid State Commun. **8**, 1397 (1988).

[15]G. Burns, C. R. Wie, F. H. Dacol, G. D. Pettit, and J. M. Woodall, Appl. Phys. Lett. **51**, 1919 (1987).

[16]M. H. Brodsky and G. Lucovsky, Phys. Rev. Lett. **21**, 990 (1968); G. Lucovsky and M. F. Chen, Solid State Commun. **8**, 1397 (1970).

[17]F. Cerdeira, C. J. Buchenauer, F. H. Pollak, and M. Cardona, Phys. Rev. B **5**, 580 (1972).

[18]T. Burnett, U. Venkateswaran, B. A. Weinstein, D. L. Smith, B. K. Laurich, and S. Subbana, Bull. Am. Phys. Soc. **35**, 763 (1990), and unpublished.

[19]S. Weissmann, J. Vac. Sci. Technol. B **4**, 1467 (1986).

[20]H. M. Kim, C. R. Wie, and C. G. Fonstad, Mater. Res. Soc. Symp. Proc. (to be published).

[21]M. Nakayama, K. Kubota, H. Kato, and N. Sano, Solid State Commun. **51**, 343 (1984).

[22]S. Yamazaki, A. Ushirokawa, and T. Katoda, J. Appl. Phys. **51**, 3722 (1980).

[23]D. L. Smith and B. K. Laurich (private communication).